Egyptian Journal of Aquatic Biology & Fisheries
Zoology Department, Faculty of Science,
Ain Shams University, Cairo, Egypt.
ISSN 1110 – 6131
Vol. 29(1): 297 – 320 (2025)
www.ejabf.journals.ekb.eg

Stratified Ocean Chlorophyll-a and Nutrient Availability in the Eastern Tropical Indian Ocean during La Nina 2022-2023

Noir P. Purba[1, 2*], Mohd Fadzil Akhir[2*], Ghelby M. Faid[3], Nur H. Roseli[2], Ignatia F. Sinaga[4], Ibnu Faizal[1]

[1]Department of Marine Science, Universitas Padjadjaran, Bandung, 40600, Indonesia
[2]Institute of Oceanography and Environment, University Malaysia Terengganu, 21030 Kuala Nerus, Terengganu, Malaysia
[3]Marine Science Study Programme, Universitas Padjadjaran, Bandung, 40600, Indonesia
[4]Komitmen Research Group, Universitas Padjadjaran, Bandung, 40600, Indonesia
[*]**Corresponding Author: noir.purba@unpad.ac.id; mfadzil@umt.edu.my**

ARTICLE INFO

Article History:
Received: Nov. 20 2024
Accepted: Dec. 25, 2024
Online: jan. 11, 2025

Keywords:
Ocean color,
Biogeochemical cycle,
Chlor-a,
Indian Ocean

ABSTRACT

This study investigated ocean productivity in the Eastern Tropical Indian Ocean (ETIO), a region defined by high biodiversity and complex interactions between physical and biogeochemical processes. This study reveals vertical patterns essential to ocean productivity by examining the dynamics of nutrients (nitrate, phosphate, and silicate) and chlorophyll-a concentrations. Nutrient data were obtained from the Copernicus Marine Service (CMEMS) with spatial resolution of 0.25° × 0.25°, concentrating on the 0–500m depth range for nitrate, phosphate, silicate, and chlorophyll-a concentrations from January 2022 to December 2023. Additional *in-situ* data were acquired from the World Ocean Database (WOD-18) utilizing quality-controlled CTD and OSD datasets, encompassing analogous nutrients in regions 3010, 3110, and 3111. According to observations, nutrient profiles show a clear nutricline at around 100 meters, where concentrations swiftly rise maximum in the subsurface. Productivity hotspots with increased phytoplankton growth are highlighted by the impact of monsoon-driven upwelling along Java's southern coast. El Niño-Southern Oscillation (ENSO)-driven seasonal changes significantly impact surface productivity, as shown by nutrient fluxes and chlorophyll-a dynamics. This study highlights how physical and chemical mechanisms shape productivity and provides crucial information for understanding how climatic variability affects marine ecosystems in the ETIO.

INTRODUCTION

Ocean productivity is often directly connected to the levels of oxygen, chlorophyll-a (Chlor-a), and nutrients in the water column **(Maradhy *et al.*, 2022)**. These productivity parameters are essential for the support of economic activities, including marine aquaculture and fishing grounds, and as indicators of ocean health **(Purba *et al.*, 2023; Makwana *et al.*, 2024)**. Additionally, these parameters are the basis of the marine food web, directly affecting the abundance and distribution of fish fisheries, which are critical

to global food security **(Maishal, 2024)**. However, understanding the variability is one of the biggest challenges in oceanography due to local and regional effects **(Tripathy *et al.*, 2020)**. Furthermore, due to disruptions in primary production and nutrient cycling, these factors have been accelerated in the context of climate change, resulting in reported decreases in ocean productivity in numerous regions **(Couespel *et al.*, 2021; Bowles *et al.*, 2024; Maishal, 2024)**.

Several factors, including local factors, riverine input and coastal dynamics, and regional phenomena influence the variability in the water column. In the tropical regions the variability is also affected by the Indian Ocean Dipole (IOD), El Niño-Southern Oscillation (ENSO), and upwelling. Recent finding found that during positive IOD phases, sea surface temperatures rise significantly, reducing nutrient availability and primary productivity, which can disrupt fisheries and marine biodiversity **(Adiwira *et al.*, 2018)**. Upwelling is frequently linked to regions with high nutrient variability due to the mixing process typically causing nutrients from the deeper layer to ascend to the surface. The concentration of nutrients, such as nitrates, generally increases significantly considerably as depth increases **(Firdaus, 2018).**

One of the complex systems in the ocean is the Eastern Tropical Indian Ocean (ETIO), which is located between the Australian continent, Timor Leste, and Indonesia. This region is a component of the eastern boundary current systems, enabling water mass transfer between subtropical and tropical regions **(Purba *et al.*, 2023)**. The primary source of the dominant water masses in this region is the Indonesian Throughflow (ITF), which originates from the Indonesian Seas. In response to atmospheric conditions such as La Niña, this region demonstrates a high degree of variability in primary productivity, particularly at the surface **(Khan *et al.*, 2024)**. Despite the significance of this parameter, the determination of biological and chemical aspects in this region has limitations for a variety of reasons: lack of *in-situ* data collection and complexity of the circulation. Furthermore, fishing locations in the Indian Ocean are frequently linked to upwelling areas, as these regions account for nearly 40% of the global fish capture **(Massel, 1999; Kasma *et al.*, 2007)**. Upwelling regions along the coastlines of Java and Sumatra consistently show chlor-a concentrations above 1 mg/m^3, indicating high primary productivity **(Horii *et al.*, 2023)**.

One of the dominant water masses in the ETIO originates from the Indonesian seas. This water mass (ITF) is essential in the regulation of the global marine environment by transporting heat and nutrient-rich water volumes from the Pacific Ocean **(Schneider, 1998; Makarim *et al.*, 2019)**. It has an impact on the productivity of marine ecosystems along its pathway, as well as regional and global climate systems and global ocean circulation **(Lee *et al.*, 2002; Sprintall *et al.*, 2014; Taufiqurrahman *et al.*, 2020)**. For instance, the nutrient-rich characteristics of these mild water masses, which have a substantial impact on marine biodiversity along their route, are underscored by the chlor-a values, which range from 0 to 4 mg/m^3, and nitrate concentrations, which range from 0

to 0.02 mmol/m³ **(Ayers *et al.*, 2014)**. Additionally, the ETIO is characterized by an exceedingly high biodiversity, which is enhanced by the presence of the Australian Great Barrier Reef, Fisheries Management Areas (FMAs 573 and 718), and Marine Protected Areas (MPA) **(Oktivana, 2023; Khan *et al.*, 2024)**. These areas preserve marine biodiversity and facilitate regional ecological balance and economic activities, including tourism and fisheries.

The purpose of this study was to investigate the productivity of the ocean in the ETIO. In order to offer a thorough knowledge of vertical productivity, this research investigated critical parameters, such as nutrient dynamics, chlor-a variability, and physical processes in this region. Additionally, in the context of climate change, numerous regions have reported a decline in ocean productivity. This study endeavoured to offer valuable insights into the dynamics of ocean productivity and its critical role in sustaining marine ecosystems, biodiversity, and economic activities by characterizing and mapping the physical and biogeochemical properties of the region. It is crucial to understand these dynamics in order to address the variability in the complex ocean system.

MATERIALS AND METHODS

1. Geographical situation

The Eastern Tropical Indian Ocean (ETIO), situated between 8 to 20^{0}S and 105 to 128^{0}E, is one of the complex ocean systems due to several phenomena (Fig 1). The complexity and variability of the Indonesian seas dynamic are highly varied due to its geographic location, sea-air interactions, and water column instability **(Sprintall *et al.*, 2014; Purba *et al.*, 2024)**.

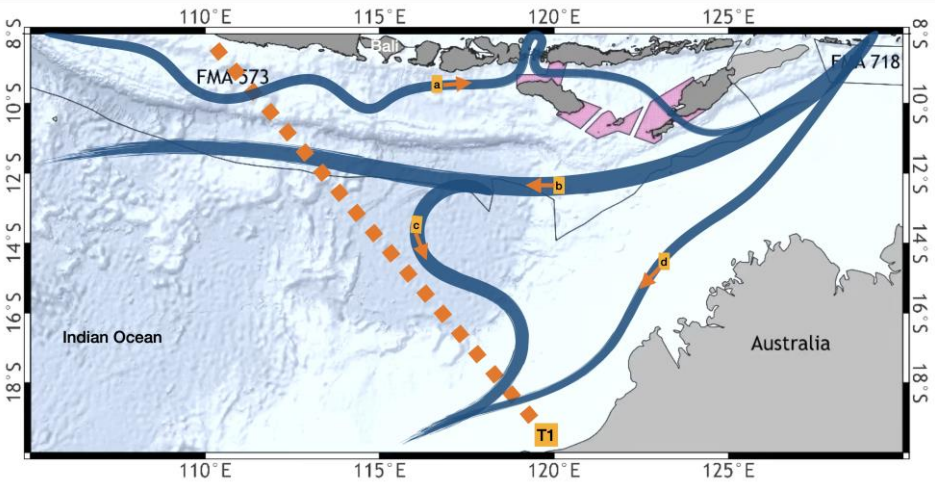

Fig. 1. Geographical map of Eastern Tropical Indian Ocean with bathymetry, MPA (orange areas), FMA 573, and FMA 718 (black lines), and continents (grey areas) as the base map. The Gridded Bathymetry Data provide the bathymetry data from GEBCO 2023 with 15 arc seconds **(GEBCO, 2023)**. Several surface currents with direction, including (a) South Java Currents, b) ITF and South Equatorial Currents, c) Eastern Gyral Currents, d) Holloway Currents. T1 (Transect 1) is sampling data from Java's coast to the Australian continent.

This region receives water mass from the Indonesian seas via the Indonesian Throughflow (ITF). Low salinity, elevated temperatures, and high concentrations of chlor-a characterize the water mass flow originating from Indonesia. This results from precipitation and river input in the Indonesian seas. Additional currents in this region comprise the South Java Currents (SJC), which traverse Java's coast to the Savu Seas. The ITF originates from multiple straits, including the Lombok Strait (LS), Savu Seas (SS), and Timor Passage (TP), and converges with the South Equatorial Currents (SEC) in the central Indian Ocean. In this region, water masses from the North Pacific Intermediate Water (NPIW) and South Pacific Intermediate Water (SPIW) were identified in the eastern Indonesian seas, primarily encompassing the Flores and Banda seas **(Gordon, 2005; Susanto *et al.*, 2021)**. The mass water flow from the northern region traverses the western coast of Australia, referred to as the Leeuwin Currents. An upwelling area exists periodically along the waters from Java to East Timor, with peaks occurring during the Australian Monsoon. June to August. Additionally, several eddies are observed in this region, resulting from the convergence of the ITF and SJC. The retroflection current from the ITF to the coast of Australia is referred to as the EGC and generates eddies. The eddies facilitate the transport of nutrients from the deeper layers to the surface layer **(Lozovatsky *et al.*, 2005; Uchida *et al.*, 2020)**.

2. Data and method

Nutrient data were obtained from E.U. Copernicus Marine Service Information (CMEMS) with a daily temporal and spatial resolution of 0.25° × 0.25° (product ID: Global_Analysisforecast_BGC_001_028). The downloaded nutrient data are mole concentration of nitrate in seawater (NO_3), mole concentration of phosphate in seawater (PO_4), mole concentration of silicate in seawater (Si), and mass concentration of chlor-a in seawater (CHL). The time range for the downloaded data is from the 1st of January 2022 to 31st of December 2023, and of the 50 available depth levels, only data in the range 0 to 500m were downloaded.

In-situ measurement data were obtained from the World Ocean Database (WOD) developed by the National Centers for Environmental Information (NCEI) and the National Oceanic and Atmospheric Administration (NOAA). This comprehensive dataset comprises information from various WOD projects. It includes high-resolution data collected through a range of instruments, such as CTD (conductivity-temperature-depth) instruments, XBT (expendable bathythermograph) probes, DRB (drifting buoy), PFL (profiled buoy), and MRB (anchor buoy) **(Boyer *et al.*, 2018)**. The dataset was updated every four years, and the latest database was published in September 2018. Detailed information about the updated database can be found in the study of **Boyer *et al.* (2018)**. The dataset chosen to obtain the same nutrient data is OSD and CTD in geographical area codes 3010, 3110, and 3111. Data quality control in this dataset was carried out using the WOD quality flag '0', which means 'accepted data' to avoid bias due to measurement errors.

3. Quality control

The WOD-18 datasets comprise *in-situ* raw data filtered to preserve only high-quality data. Quality control for this comprehensive profile dataset is crucial to enhance the precision of the results. Consequently, many procedures were undertaken prior to analysis, as detailed below: 1) Extracting the necessary data, encompassing temperature, salinity, oxygen, longitude, latitude, depth, and date within the specified spatial and temporal parameters; 2) identifying outliers and excluding data outside the temperature range of 0 to 35°C and salinity range of 20 to 40psu; 3) eliminating stations with fewer than three values in the vertical dimension; and 4) developing a database from observed levels to standardized depths **(Purba *et al.*, 2021)**. The weighted-average gridding interpolation method was used in scalar values, and XBT/MBT corrections were done using the data presented in the study of **Cheng *et al.* (2014)**.

The more complete data on temperature and salinity can be found in Table (1). The data provides a statistical summary of the primary water quality parameters (NO_3, PO_4, Si, and Chl) in three depth ranges: 0 to 50m, 51 to 150m, and 151 to 500m. The distribution and variability of the data are described by calculating the mean, minimum, maximum, standard deviation, and standard error for each parameter.

Table 1. Statistical overview of nutrient and chlor-a concentrations by depth layers

Depth	Variable	Mean	Min	Max	Std. dev	Std. Error
0-50	NO_3	0.040	0	15	0.431	0.0004
	PO_4	0.083	0.019	1.5	0.043	0
	Si	2.846	0.914	35	0.524	0.0005
	Chl	0.169	0.003	1.5	0.178	0.0001
51-150	NO_3	4.756	0	15	4.568	0.0075
	PO_4	0.458	0.019	1.5	0.312	0.0005
	Si	6.754	0.914	35	4.889	0.0081
	Chl	0.333	0.003	1.5	0.181	0.0002
151-500	NO_3	20.065	0	15	6.325	0.0099
	PO_4	1.432	0.019	1.5	0.396	0.0006
	Si	27.474	0.914	35	10.712	0.0167
	Chl	0.022	0.003	1.5	0.026	0

At the surface layer (0 to 50 m), nitrate (NO_3) exhibits a low mean of 0.040µmol/L, with values ranging from 0 to 15µmol/L and a standard deviation of 0.431µmol/L,

suggesting minimal variability. The mean phosphate concentration (PO4) is 0.083 µmol/L, while the average silicate (Si) concentration is 2.846 µmol/L. In these layers, the mean concentration of chlor-a, which is a metric for primary productivity, is 0.169µg/ L. Nutrient concentrations substantially increased in the mid-depth stratum (51 to 150m). The standard deviation of 4.56µmol/ L indicates greater variability as the mean nitrate level increases to 4.756µmol/ L. Silicate and phosphate concentrations have also increased, with an average of 6.754µmol/ L and 0.458µmol/ L, respectively. Nutrient levels reach their maximum in the deeper layers (151 to 500m). Nitrate exhibits substantial variability, with a mean of 20.065µmol/ L and a high standard deviation of 6.325µmol/ L. The phosphate and silicate are also elevated, with a value of 1.432µmol/ L and 27.474µmol/ L, respectively. In contrast, the mean chlor-a concentration decreases significantly to 0.022µg/ L. The standard deviations and errors suggest that there is variability across all strata, with the most significant fluctuations in nitrate and silicate concentrations occurring in deeper waters.

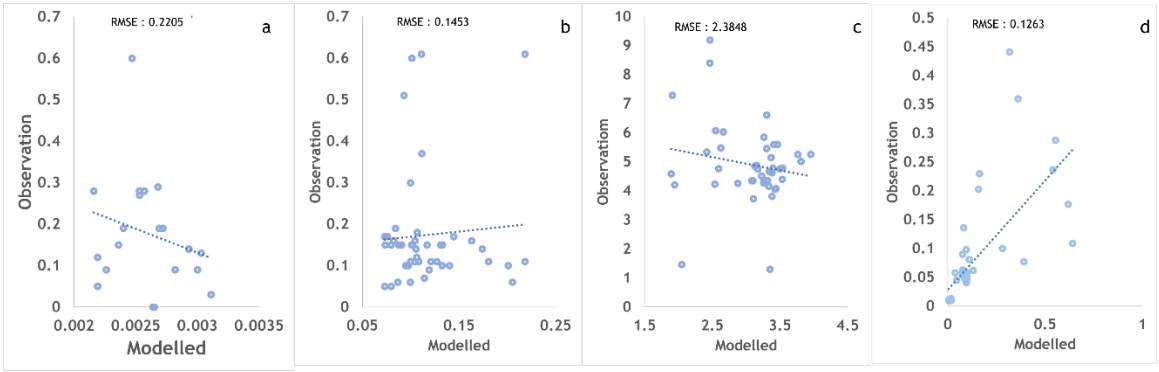

Fig. 2. RMSE value between modeled and *in-situ* data for a. Nitrate; b. Phosphate; c. Silicate; and d. Chlor-a

The RMSE value for NO_3 is 0.2205mmol m^{-3}, indicating a moderate level of error between the modeled and observed data. This means that the model performs reasonably well in predicting NO_3 concentrations, although there may be room for improvement, especially in areas where nitrogen dynamics play a critical role, such as nutrient-driven biological processes. For PO_4, the RMSE is 0.1453mmol m^{-3}, which is quite low compared to the other variables. This would then imply a better model accuracy for phosphate concentrations. Phosphate usually does not vary highly in open ocean conditions, which may explain the stronger performance of the model in predicting this nutrient.

The RMSE of Si increases to a larger value: 2.3848 mmol m^{-3}. The large skill error indicates that the model is badly parameterizing the silicate dynamics, which are normally more complex and have strong regional variations. Variability, including diatom blooms, river inputs, and several remineralization processes, contributes to such

deviation. Improvement in silicate-related processes by the model could hence reduce this error. Finally, the RMSE for Chl is relatively small, 0.1263mg m^{-3}, compared with the nutrient variables. This suggests that the model's performance is relatively very good in predicting chlor-a concentrations. This could probably be explained by the fact that chlor-a is itself often derived using satellite data or empirical algorithms, which, in any case, tend to agree closely with observed data.

The RMSE value for NO_3 is 0.2205mmol m^{-3}, indicating a moderate level of error between the modelled and observed data. This means that the model performs reasonably well in predicting NO_3 concentrations, although there may be room for improvement, especially in areas where nitrogen dynamics play a critical role, such as nutrient-driven biological processes. For PO_4, the RMSE is 0.1453mmol m^{-3}, which is quite low compared to the other variables. This would then imply a better model accuracy for phosphate concentrations. Phosphate usually does not vary highly in open ocean conditions, which may explain the stronger performance of the model in predicting this nutrient.

The RMSE of Si increases to a larger value: 2.3848mmol m^{-3}. The large skill error indicates that the model is badly parameterizing the silicate dynamics, which are normally more complex and have strong regional variations. Variability including diatom blooms, river inputs, and several remineralization processes contributes to such deviation. Improvement in silicate-related processes by the model could hence reduce this error. Finally, the RMSE for Chl is relatively small, 0.1263mg m^{-3}, compared with the nutrient variables. This suggests that the model's performance is relatively very good in predicting chlor-a concentrations. This could probably be explained by the fact that chlorophyll is itself often derived using satellite data or empirical algorithms, which, in any case, tend to agree closely with observed data.

4. Analysis

Ocean Data View (ODV) **(Schlitzer, 2024)** and QGIS were used to process data ranging from filtering data to vertical visualization of the study area. Both of these tools have powerful data processing capabilities, so they can produce visualizations to support analysis. A transect with five points along the transect was chosen as representative for identifying water mass types. The T-S diagram is used to identify the type and origin of water masses in the transect based on the study of **Emery (2001)**. The T-S time was determined using salinity and potential temperature according to TEOS-10. A T-S diagram displays the potential temperature on the vertical axis against salinity on the horizontal axis, incorporating density for two distinct seasons. The density values were derived from each dataset utilizing the equation of state for seawater.

The analysis of vertical productivity in the ETIO utilized nutrient concentration data (nitrate, phosphate, and silicate) and chlor-a measurements across various depth layers. Chlor-a, an indicator of phytoplankton biomass, was examined in conjunction with nutrient data to evaluate trends in primary production. The data were analyzed to

investigate the impact of environmental conditions, including upwelling and nutrient mixing, on productivity. Statistical methods were utilized to illustrate vertical gradients and to associate productivity trends with nutrient availability.

RESULTS

1.Temperature, salinity, and oxygen characteristics

The analysis highlights seasonal temperature, salinity, and oxygen concentrations variations in the ETIO region (Fig. 3).

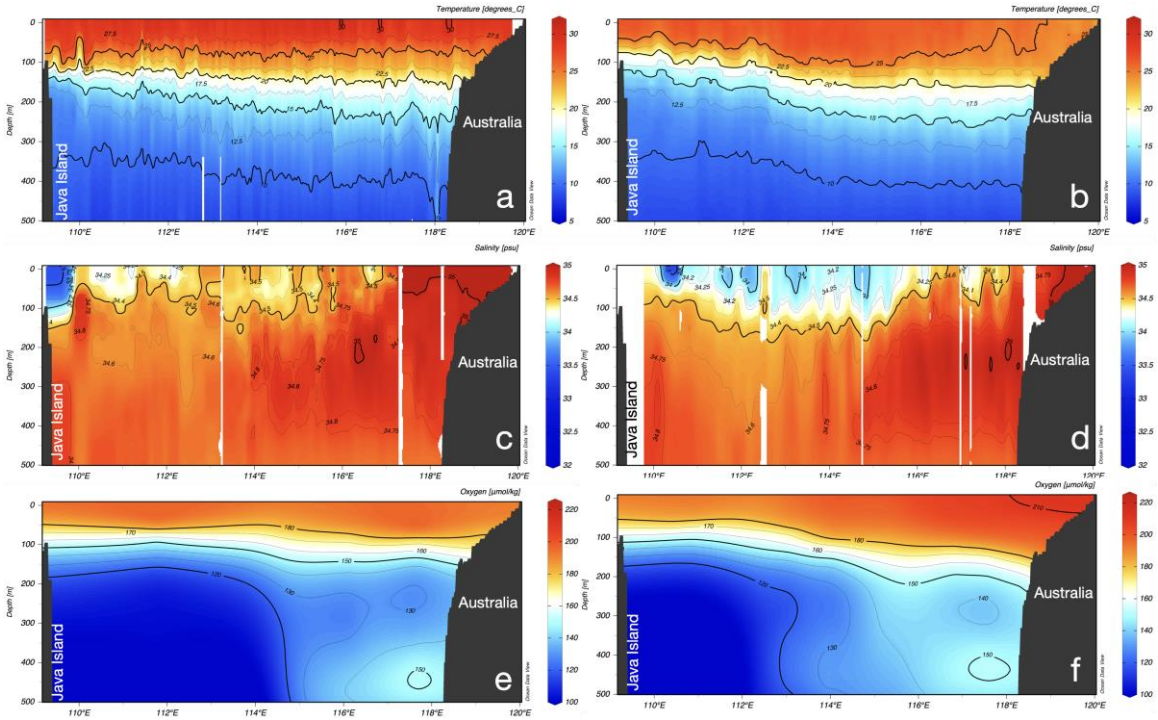

Fig. 3. Vertical temperature (a,b), salinity (c,d), and oxygen (e,f) in northwest monsoon (left panels) compared to southeast monsoon (right panels)

During the northwest monsoon, surface temperatures at depths of 0 to 100m vary from 28 to 30°C, with a peak in the eastern region. A significant decrease to 15°C found at 100 to 200m in the western region (Fig. 3a). However, the eastern part exhibits a more dynamic decline. At depths below 200m, temperatures are stable between 4 and 5°C in all locations. During the southeast monsoon, surface temperatures are slightly lower, fluctuating between 27 to 29°C, with the peak values occurring in the western part of the region (Fig. 3b). The most significant decrease in temperature occurs at depths of 50 to 150m, reaching 15°C in the west, whereas the eastern temperatures reduce more gradually. At depths exceeding 150 meters, temperatures are reliably stable at 4°C. Salinity trends exhibit significant variations between the two seasons. During the northwest monsoon, surface salinity (0 to 50 m) varies from 33 to 35psu, with the western region showing the lowest values (33 to 34.5 psu) and the eastern region recording the

highest (35psu) (Fig. 3c). At depths of 50 to 150m, salinity reveals a slight increase in the west (33 to 34.6psu) while remaining fairly uniform in the center (34.5 to 34.8psu) and in the eastern region (34.9 to 35psu). Salinity has similar characteristics at depths below 150m, with the western region at 34.5 to 34.6psu, the central region at 34.6 to 34.8 psu, and the eastern region at 34.9 to 35psu. Salinity levels at 0 to 50m depths are comparable during the southeast monsoon. Nevertheless, there is a wider distribution of low salinity, especially in the western (33 to 34psu) and central (33.8 to 34.5psu) regions. Salinity rises across all zones at 50 to 150 m depths, varying from 34.3 to 34.6psu in the west and center to 34.5 to 35psu in the eastern region (Fig. 3d).

Oxygen concentrations exhibit seasonal fluctuation as well. During the northwest monsoon, surface oxygen concentrations (0 to 50m) range from 180 to 190µmol/ kg, with slight regional variation (Fig. 3e). At depths of 50 to 100m, oxygen concentrations diminish to 150 to 180µmol/ kg, with a constant decrease below 100m, reaching 100 to 150µmol/kg in the west and 130 to 150µmol/ kg in the east. During the southeast monsoon, surface oxygen levels (0 to 50m) are elevated, ranging from 180 to 200 µmol/kg, with a peak in the eastern region. At depths of 50 to 100m, oxygen levels decrease to 160 to 180µmol/ kg in the west, 170 to 180µmol/ kg in the center, and 180 to 190µmol/ kg in the east (Fig. 3f). Oxygen concentrations below 100m stable around 100 to 160µmol/ kg in the west, 120 to 170µmol/ kg in the center, and 140 to 180µmol/ kg in the east.

Furthermore, several water masses were found in this region. There are 8 types of water masses originating from the Indian Ocean, spread from the upper to deep waters, while the other 6 were identified as originating from the Pacific Ocean, which was only identified in the upper waters (Fig. 4).

In upper waters, the types of water masses found are Bengal Bay Water (BBW), Indian Equatorial Water (IEW), Indonesian Upper Water (IUW), South Indian Central Water (SICW), Western North Pacific Central Water (WNPCW), Eastern North Pacific Central Water (ENPCW), Pacific Equatorial Water (PEW), Western South Pacific Central Water (WSPCW), Eastern South Pacific Central Water (ESPCW), and Eastern South Pacific Transition Water (ESPTW). In intermediate waters, three types of water masses have been identified, namely Antarctic Intermediate Water (AAIW), Indonesian Intermediate Water (IIW), and Red Sea Persian Gulf Intermediate Water (RSPGIW). Meanwhile, only Circumpolar Deep Water (CDW) is found in deep waters.

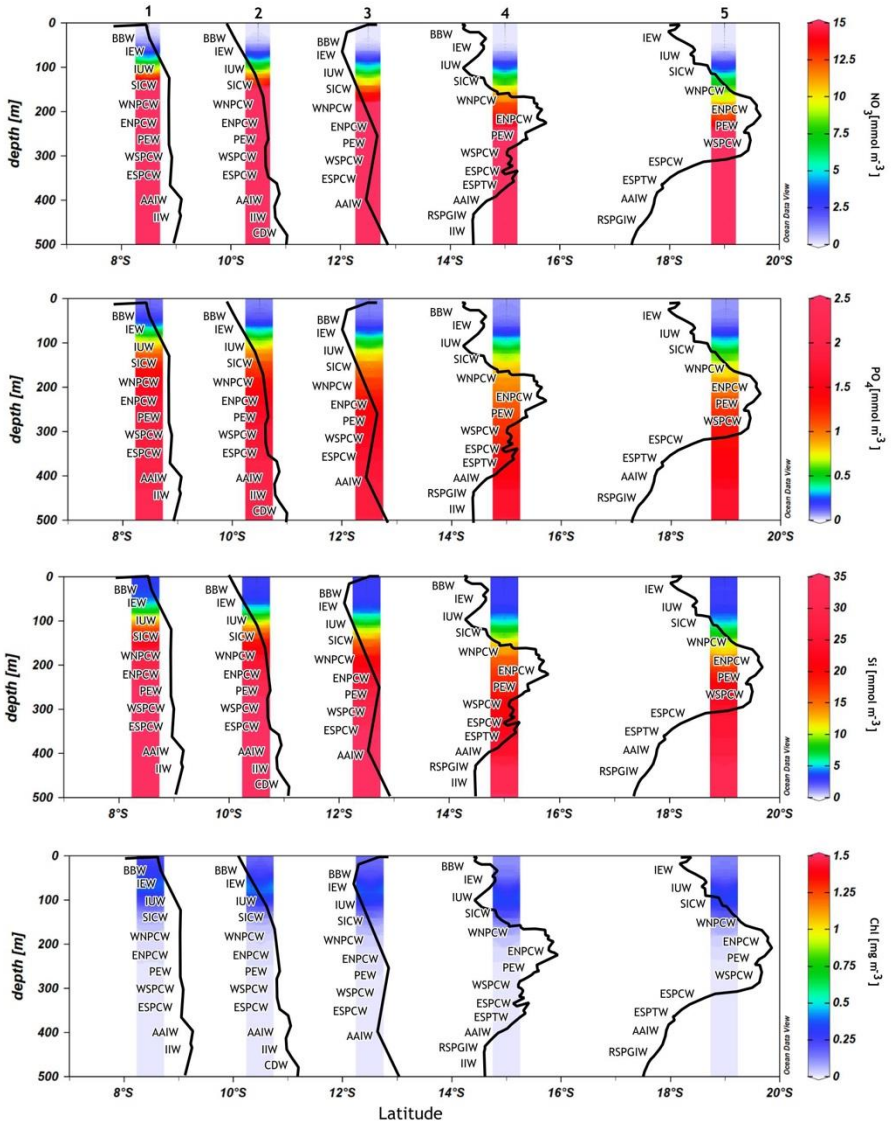

Fig. 4. Vertical profiles of nitrate, phosphate, silica, and chlor-a at five points along the transect with an overlay of T-S diagram lines and water mass types

In the upper waters layer, points 1, 2, and 3 have the same type of water mass: BBW, IEW, IUW, SICW, WNPCW, ENPCW, PEW, WSPCW, and ESPCW. Point 4 is generally identified as having the same water mass as the previous three points with the addition of ESPTW, so it has 10 types of water mass. Meanwhile, point 5 has nine types of water masses with the same structure as points 1, 2, and 3, but there is ESPTW and no BBW. In the intermediate waters layer, points 1 and 2 are both identified as having AAIW and IIW. Point 3 was only identified as having AAIW. Meanwhile, points 4 and 5 were identified as having AAIW and RSPGIW. In the deep waters layer, only point 2 was identified as having a water mass type from this category, namely CDW.

The temperature and salinity profile pattern at point 1 is quite similar to point 2, with a temperature range between 5 & 27.5℃ at both points and a salinity range from

33.7 to 34.7 at point 1 and slightly narrower at point 2, namely from 34.2 to 34.7. Point 3 has its own distinctive pattern with a temperature range from 7.5 to 27.5℃ and a salinity range from 34.4 to 34.75. Points 4 and 5 have a fairly similar salinity range, namely from 34.5 to 35.4, while the temperature range at these two points is 5 to 29.8℃ and 7.5 to 25℃, respectively.

2. Nutrient profile

The vertical nutrient profile based on latitude has the same characteristics for the four variables, and the nutricline is found at a depth of around 100m (Fig. 5). In the nitrate variable, the value changes drastically from 0.1 to 7.5mmol m^{-3}. Phosphate changed from 0.08 to 0.75mmol m^{-3}. Silica doubled from 5 to 10mmol m^{-3}. Meanwhile, chlor-a increased from 0.15 to 0.5 mg m-3. Apart from the same nutricline depth, three variables – nitrate, phosphate, and silicate – also have the same pattern: higher variable values at lower latitudes, from 8 to 14 °S.

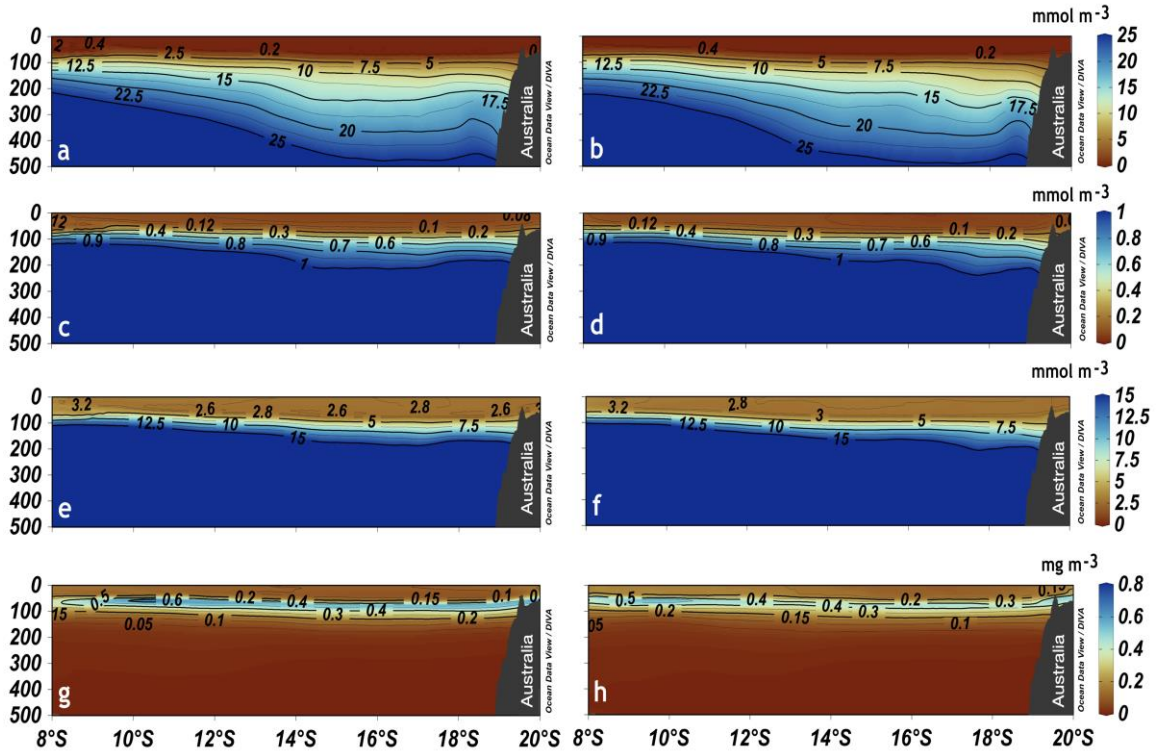

Fig. 5. Vertical profile in NWM (Left Figs.) and SEM (Right Figs.) of nitrate (a,b), phosphate (c, d), silica (e, f), and chlor-a (g, h) along the transect

On the surface, nitrate can reach up to 15 mmol m^{-3} at a depth of around 130 m and below (Fig 5a). Depth 0 to 50 has a low value of around 0.3 mmol m^{-3} with a distribution pattern that gets deeper as latitude increases. This value changes drastically to 7.5 mmol m^{-3} in the nutricline layer at a depth of about 100m at all latitudes. The profile of nitrate values below this layer has a narrower stratification depth at lower latitudes. In the area between 8 & 10°S, nitrate values from 7.5 to 15mmol m^{-3} changes in a shallow depth

range of less than 120m. Meanwhile, in the area between 14 & 18°S, nitrate values of 15mmol m^{-3} occur at deeper depths, around 200m.

Phosphate values in the transect range from 0.1mmol m^{-3} at the surface to 1.5 $mmolm^{-3}$ at a depth of around 450 m (Fig 5d). Phosphate levels less than 0.2mmol m^{-3} predominate over 0 to 50m depths. This value exists in depths of no more than 25m in lower latitudes and in deeper depths of roughly 50m in higher latitudes. Along the transect, the nutricline layer exists at approximately 100m, where the phosphate value rises from 0.12 to 0.75mmol m^{-3}. At a depth of less than 200m in a location at latitude 8°S, 1.5mmol m-3 showed the highest phosphate value on the transect. This number was found 350m in the area near latitude 14°S. This value is also observed at a more than 400m depth at latitude 20°S.

The silicate value in the transect ranges from 0 to 35mmol $m^{-3,}$ with a value of 5mmol m^{-3} dominating the surface water column. The nutricline is at a depth of approximately 100m with a change in silicate value from 3.5 to 10mmol m^{-3}. Similar to the previous two variables, areas at lower latitudes have dense stratification at lower depths (Fig. 5e). It can be seen that in the area at latitude 8°S, the phosphate value of 3.5mmol m^{-3} is around 50m, while in the area at latitude 19°S, this value is found at a depth approaching 100m. In fact, a very striking difference was seen in the phosphate value of 30mmol m^{-3} identified at a depth of around 200m at latitude 8°S.

The chlor-a value in the transect ranged from 0 to 1.5mg $m^{-3,}$ with the highest value at a depth of around 50m (Fig. 5g). The identified surface water column is dominated by a chlor-a value of 0.15mg m^{-3}. The highest chlor-a was identified at depths of 0 to 100m with values of 0.25 to 1.5mg m^{-3}. This chlor-a-rich layer is consistently at the same relative depth along the transect with the exception of the initial and final areas of the transect, where this layer occurs starting from a depth of 0m while in other areas starting from a deeper depth. The chlor-a value below this layer, starting from a depth of around 150m, continues to decrease with increasing depth.

The vertical profile of nutrients based on the month of data collection (Fig. 6) shows a relatively stable condition for all nutrients except chlor-a. The vertical profile has a different distribution due to the chlor-a-rich layer rising to the surface from July to September. The nutricline layer can be located at a depth of around 100m in all months.

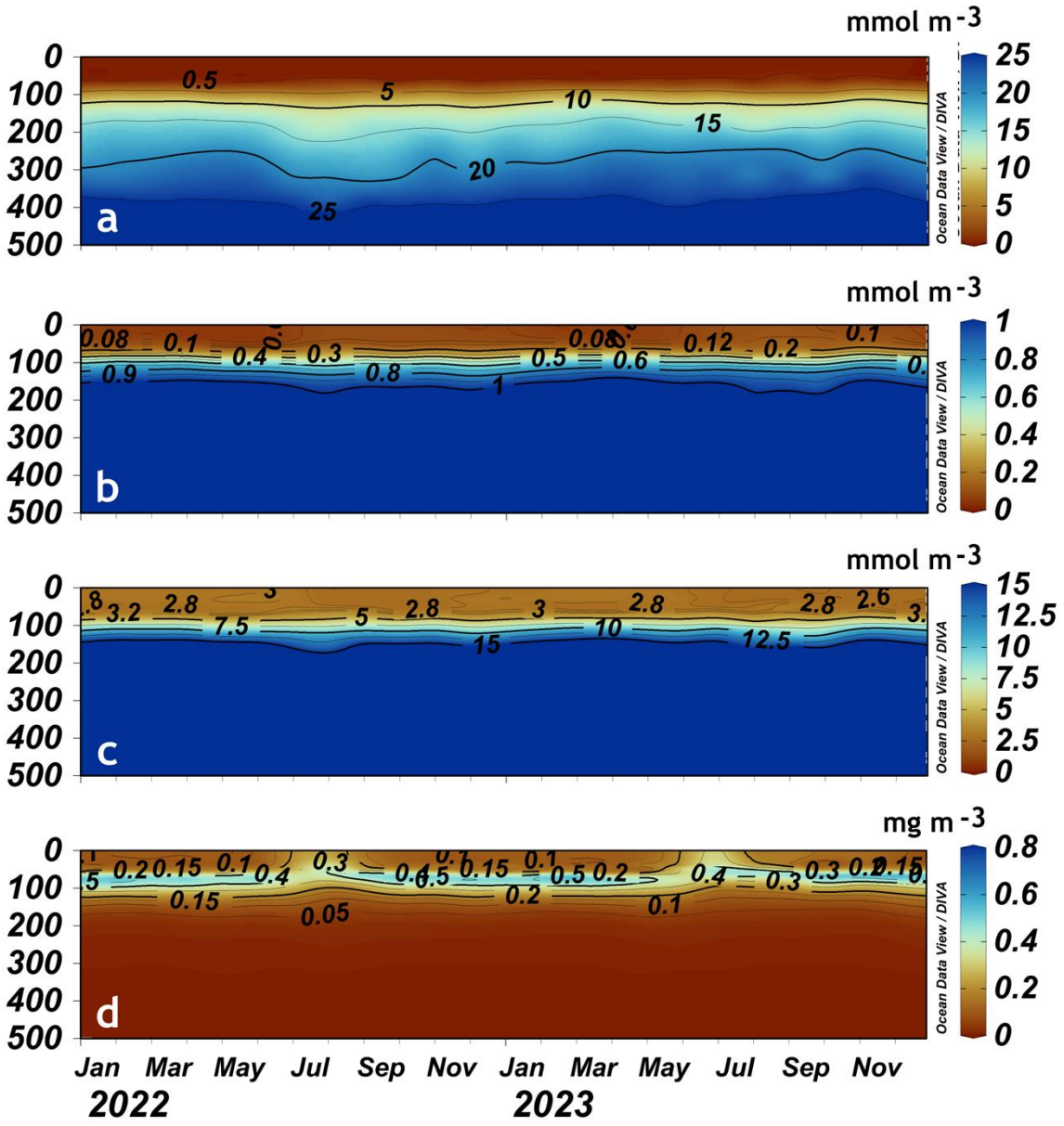

Fig 6. Vertical profile of a) nitrate, b) phosphate, c) silica, and d) chlor-a along the transect based on the month of data collection

The nitrate profile had a stable stratification throughout the month. The layer from the surface to 200m has heterogeneous stratification, while the layer below has homogeneous stratification (Fig. 6a). The value of 0.2mmol m^{-3} dominates at a depth of 0 to 50m, followed by a nutricline layer approximately 50m thick, where the nitrate value increases drastically to 7.5mmol m^{-3}. The highest value, 15mmol m^{-3}, is stable at a depth of about 200m. Similar to nitrate, phosphate values tend to be stable from the first month to the last. A 0 to 75m depth has a homogeneous phosphate level of around 0.1mmol m^{-3}. The nutricline layer where the nitrate value increases from 0.1 to 0.5mmol m^{-3} in this variable is thinner, compared to nitrate, with a thickness of around 25m (Fig. 6b). In the

water column below this layer, up to around 300m, the identified phosphate value is between 0.75 to 1.5mmol m^{-3}. Meanwhile, in the water column deeper than 300m, the phosphate value is around 1.5mmol m^{-3}. The vertical silicate profile has slightly different characteristics than the previous two variables. The homogeneous surface layer on this variable has a thickness of almost 100m, with a silicate value range of 0 to 3.5 mmol m^{-3}. The nutricline layer in this variable is also located deeper, around 100 to 125m, where the silicate value increases drastically from 3.5 to 15mmol m^{-3} (Fig. 6c). Depths of 150 to 300 m were identified as having silicate values ranging from 15 to 25mmol m^{-3}. The highest silicate values identified were at intermediate depths with fluctuating starting points from 300 to 350m. The vertical profile of chlor-a based on the month of data collection has a quite unique pattern where in the first 6 months and the last 3 months, the 0 to 50m water column had a chlor-a value of less than 0.2mg m^{-3}. Meanwhile, from July to September, the water column was identified as having a value of around 0.3 to 0.4mg m^{-3}, which generally occurs at depths between 50 to 125m (Fig. 6d). The chlor-a-rich layer is at a depth of 50 to 125m with a value range of 0.3 to 0.4 mg m^{-3}. Chlor-a conditions at more than 200m depths are homogeneous, with chlorophyll values of less than 0.1mg m^{-3}.

3. Nutrient and chlorophyll-a dynamics during La Nina

This dataset presents a thorough examination of the concentrations of chlor-a (Chl), nitrate (NO_3), phosphate (PO_4), and silicate (Si), as well as the Oceanic Niño Index (ONI), over a two-year period from January 2022 to December 2023. The ONI values are a measure of the state of the El Niño-Southern Oscillation (ENSO). La Niña conditions are represented by negative values such as -1 and -0.9, while El Niño conditions are represented by positive values such as 1.8 and 2. These values are indicative of the oceanic and atmospheric interactions that have a substantial impact on marine ecosystems (Fig. 7).

Variability in chlor-a values for 24 months from 1 January 2022 to 31 December 2023 on the surface (fig. 7a) shows that there are two spikes. In September 2022, the chlor-a value increased to around 0.5mg m-3. Then, in September 2023, a large increase of more than 0.5mg m-3 was detected. Meanwhile, at depths of 150 (fig. 7b) and 300 (fig. 6 c), the chlor-a value is very stable. There is no significant increase or decrease. The three variability graphs are overlaid with the Ocean Niño Index (ONI) over the same time span. The ONI value from January 2022 to February 2023 is in the minus phase, which is a sign of La Niña. Meanwhile, from February to December 2023, ONI is in a positive phase, which is an indicator of El Niño.

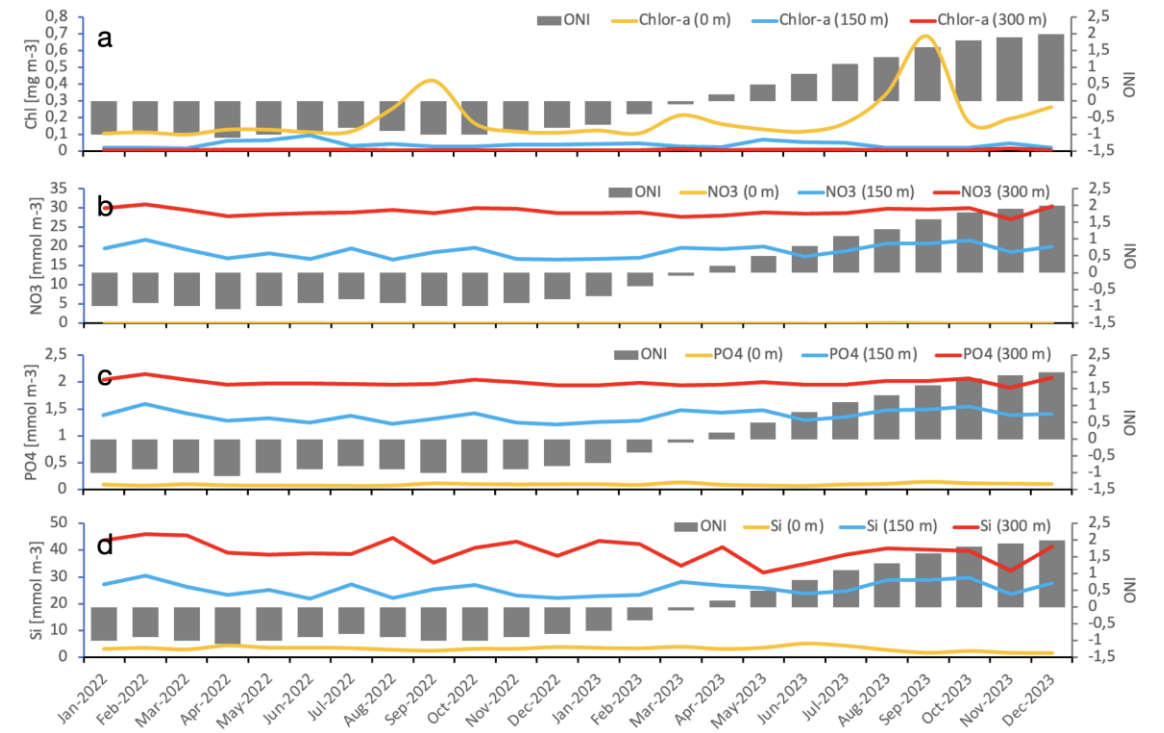

Fig. 7. Chlorophyll-a time series profile in the 2022 - 2023 time period with Ocean Niño Index overlay at a. surface; b. 150m; and c. 300m

On the surface, it is evident from the data that chlor-a concentrations, which function as a proxy for marine primary productivity, exhibit seasonal fluctuations. In September 2023, the maximum concentrations of chlor-a were recorded (0.6861 mg/m³), which coincided with a positive ONI value of 1.6, indicating that productivity was higher during El Niño conditions. In March 2022, the ONI values were negative, which is indicative of La Niña conditions, resulting in lesser values (0.09919mg/ m³). The nutrient availability dynamics, regulated by the temperature and currents that fluctuate during ENSO events, are likely to influence these variations in chlor-a levels. The highest nitrate (NO_3) concentrations were recorded in March 2023 (0.01367 mmol/m³), when the ONI value was nearly neutral (-0.1), suggesting a transition phase between La Niña and El Niño. Nitrate concentrations are essential for maintaining marine productivity, as they are a critical nutrient for phytoplankton. Phosphate (PO_4) and silicate (Si) levels exhibited comparable patterns, with significant the maximum in specific months, including March 2023 (0.13847 mmol/m³) for phosphate and July 2023 (5.23149 mmol/m³) for silicate.

In the 150m, it is evident from the data that chlor-a concentrations, which function as a proxy for marine primary productivity, exhibit seasonal fluctuations. In September 2023, the maximum concentrations of chlor-a were recorded (0.6861 mg/m³), which coincided with a positive ONI value of 1.6, indicating that productivity was higher during El Niño conditions. In March 2022, the ONI values were negative, which is indicative of La Niña conditions, resulting in a lower value (0.09919mg/ m³). The nutrient availability

dynamics, regulated by the temperature and currents that fluctuate during ENSO events, are likely to influence these variations in chlor-a levels. The highest nitrate (NO_3) concentrations were recorded in March 2023 (0.01367 mmol/m³), when the ONI value was nearly neutral (-0.1), suggesting a transition phase between La Niña and El Niño. Nitrate concentrations are essential for maintaining marine productivity, as they are a critical nutrient for phytoplankton. Phosphate (PO_4) and silicate (Si) levels exhibited comparable patterns, with significant the maximum in specific months, including March 2023 (0.13847 mmol/m³) for phosphate and July 2023 (5.23149 mmol/m³) for silicate.

In 300 m, Chl-a, a critical indicator of primary productivity, exhibits fluctuations throughout the period, with the highest values occurring in March 2023 (0.01558mg/ m³) and November 2023 (0.01597mg/ m³). These higher concentrations may indicate an increase in biological activity, which may be influenced by the altering nutrient concentrations or shifts in ENSO conditions. This is due to the fact that the ONI values are approaching positive values during these months, reaching 1.9 in November 2023. The concentrations of nitrate (NO_3) follow a similar pattern, with higher values observed in February 2022 (30.96mmol/ m³) and December 2023 (30.48mmol/ m³). This indicates that nutrient availability is abundant during specific periods. Potential upwelling and biological consumption processes are consistent with nitrate levels' modest decline during positive ONI phases, as evidenced by the values of 27.6mmol/ m³ in March 2023 and 27.04mmol/ m³ in November 2023. Phosphate (PO_4) exhibits comparatively consistent behavior throughout the duration, fluctuating between 1.89mmol/ m³ (in November 2023) and 2.14mmol/ m³ (in February 2022). These variations are typically associated with nutrient cycling in the ocean, where phosphate is a significant limiting factor for phytoplankton growth. Similarly, nutrient availability is reflected in silicate (Si) concentrations, which vary from 31.54mmol/ m³ in May 2023 to 46.01mmol/ m³ in February 2022. This is particularly true for diatom species; whose productivity is contingent upon silicate to construct their skeletons.

DISCUSSION

From the result, the vertical distribution of phytoplankton in the water column is significantly influenced by the depth of the mixed layer, the strength and depth of the pycnocline, the stratification of water column temperature and salinity (density) (Fig. 3) **(Prairie *et al.*, 2012).** The findings reveal distinct vertical stratification in nutrient concentrations, aligning with the oceanographic processes in this region **(Purba *et al.*, 2024).** In the surface layer, nitrate concentrations are notably low at 0.3 mmol m^{-3}, indicate of nutrient depletion in the photic zone due to active uptake by phytoplankton during photosynthesis **(Maradhy *et al.*, 2022).** Corresponding with the nutricline, nitrate concentrations rise significantly to 7.5mmol m^{-1} at a depth of 100m, indicating a strong gradient which nutrients are supplied from deeper waters. This sharp transition

underscores the critical role of vertical mixing and upwelling in modulating nutrient availability at the surface **(Paul *et al.*, 2022)**.

Similarly, phosphate concentrations exhibit a comparable vertical gradient, with levels less than 0.2mmol m^{-3} in the upper 50m, increasing to 0.75mmol m^{-3} at the nutricline (100m) and further to 1.5mmol m^{-3} at 200m. These trends highlight the importance of phosphate in supporting deeper biogeochemical processes and suggest potential nutrient limitation in the upper layers, which could influence primary production and ecosystem dynamics **(Duhamel *et al.*, 2016)**. The vertical distribution of silicate shows distinct variability, with concentrations of approximately 5mmol m^{-3} at the surface and increasing to 10mmol m^{-3} at the nutricline at 100m. This gradient emphasizes the function of silicate as a limiting nutrient for diatoms, a dominating group of phytoplankton depending on silicate for frustule production. Important for maintaining diatom output in the area, the greater silicate concentration near the nutricline indicates remineralization processes and nutrition supply from deeper layers (**Kamalanathan *et al.*, 2021)**. The observed silicate concentration at the surface suggests moderate nutrient availability, which could support limited diatom growth depending on the interplay with other nutrients, such as nitrogen and phosphate. The increase in silicate concentrations at the nutricline demonstrates the importance of physical processes, such as vertical mixing or upwelling, in supplying silicate to surface waters. In regions where such processes are active, silicate availability could fuel diatom blooms, contributing significantly to primary productivity (Fig. 5). Conversely, in the absence of effective mixing, silicate limitation may constrain the productivity of siliceous phytoplankton, potentially altering the structure of the phytoplankton community.

In the photic zone (near-surface waters, 0 to 3m), the low nitrate concentration (0.3 mmol m^{-3}) is typical of nutrient-depleted conditions driven by biological uptake. Phytoplankton, the primary producers in marine ecosystems, utilize available nitrogen and phosphate to grow and reproduce during photosynthesis. This rapid nutrient consumption often leads to oligotrophic conditions, especially in tropical and subtropical regions where nutrient is limited. Phosphate concentrations, also follows a similar depletion pattern in surface waters (< 0.2mmol m^{-3}). Phosphate is a critical macronutrient for cellular functions, including synthesis and membrane formation in phytoplankton. The depletion of nitrogen suggests active biological cycling and potential nutrient limitation for primary producers. Such limitations can constrain productivity, particularly in regions where nutrient from deeper waters is limited **(Bristow *et al.*, 2017)**.

The dramatic increase in nitrate concentrations from 0.3 mmol m^{-3} at the surface to 7.5 mmol m^{-3} at 100 m highlights the presence of a well-defined nutricline. This zone represents a transition layer where nutrient concentrations increase sharply due to reduced biological uptake and active replenishment from deeper water masses. The sharpness of this gradient reflects the intensity of nutrient transport processes, such as upwelling and vertical mixing (Fig. 4). These physical processes bring nutrient-rich deep water to the

surface, supporting phytoplankton blooms and enhancing primary production **(Tanaka *et al.*, 2021)**.

Similarly, the increase in phosphate concentrations from < 0.2mmol m^{-3} at 50m to 0.75mmol m^{-3} at 100m and further to 1.5mmol m^{-3} at 200m suggests a strong contribution from remineralization processes. Organic matter sinking from the surface at the deeper layer undergoes microbial decomposition, releasing nitrogen, phosphate, and other nutrients into the water column. This vertical cycling is crucial for maintaining nutrient availability in deeper layers, which can then be redistributed to the surface under favorable conditions. These nutrient profiles indicate a system where vertical nutrient transport is a key driver of productivity. The low surface nutrient concentrations suggest that the region may experience oligotrophic conditions, which could limit primary productivity. However, the presence of a well-defined nutricline indicates that with sufficient physical processes, such as upwelling or mixing, nutrients can be brought to the surface to sustain phytoplankton growth **(Labiosa *et al.*, 2003)**.

The distinct vertical stratification of nitrate and phosphate highlights the interplay between nutrient availability and primary productivity. Surface nutrient depletion and the sharp nutricline suggest that phytoplankton growth in the ETIO may be constrained by nutrient availability. However, the presence of a well-defined nutricline indicates that productivity could be rapidly enhanced if vertical mixing or upwelling occurs, bringing these nutrients into the photic zone **(Khan *et al.*, 2024)**. Furthermore, ocean currents in the Eastern Indian Ocean are essential for transporting nutrients throughout the area. By enriching coastal and pelagic ecosystems with nutrients, these currents promote primary productivity and sustain intricate food webs. The movement of nutrient-rich water masses from the Pacific to the Indian Ocean, for instance, is facilitated by the Indonesian Throughflow (ITF), which might improve biological productivity in ETIO **(Sprintal *et al.*, 2014)**. This dynamic balance between nutrient uptake, vertical transport, and remineralization processes underscores the complexity of nutrient cycling in ocean systems. Regions with limited mixing are likely to support oligotrophic ecosystems dominated by small, slow-growing phytoplankton, whereas areas with active mixing could sustain blooms of larger, fast-growing species, such as diatoms, which rely heavily on both nitrogen and phosphate.

The chlor-a distribution reflects the spatial variability in phytoplankton biomass and productivity. Surface chlor-a concentrations are dominated by values around 0.15 mg m^{-3}, indicating relatively low phytoplankton biomass in the photic zone. However, within the 0 to 100 m depth range, chlor-a values increase significantly, reaching 0.25 to 1.5 mg m^{-3}. This pattern suggests the presence of a subsurface chlor-a maximum (SCM), a feature commonly observed in tropical and subtropical oceanic regions. The SCM is typically associated with enhanced nutrient availability near the nutricline, where light levels remain sufficient to support photosynthesis. The gradual decrease in chlor-a concentrations below 100 m reflects the diminishing light availability and the subsequent

decline in photosynthetic activity **(Sarkar *et al.*, 2021; Khan *et al.*, 2024)**. This vertical pattern is consistent with the photic zone's boundaries and the nutrient-driven dynamics influencing phytoplankton growth. The SCM observed in this study underscores the critical role of nutrient stratification and light availability in shaping the vertical distribution of phytoplankton biomass.

The co-occurrence of elevated silicate concentrations and higher chlor-a values near the nutricline highlights the potential for nutrient-driven phytoplankton productivity in the ETIO. Diatoms, which rely heavily on silicate, may dominate the phytoplankton community near the SCM, leveraging the enhanced nutrient availability at this depth. This relationship between silicate and Chl-a underscores the importance of nutrient dynamics in determining the composition and productivity of phytoplankton communities. The observed nutrient profiles emphasize the importance of vertical mixing and upwelling in modulating nutrient distributions. Regions with active upwelling, such as coastal zones or areas influenced by ocean currents, tend to have higher surface nutrient concentrations due to the upward transport of nutrients from depth. In contrast, areas with strong stratification, as commonly observed in tropical waters, may experience limited nutrient flux, leading to reduced productivity. Understanding the mechanisms governing nutrient transport in the ETIO is essential for predicting productivity hotspots and their variability under changing climatic conditions **(Ayers *et al.*, 2014)**.

In the ETIO, upwelling intensity is closely linked to monsoonal wind patterns **(Lahiri & Vissa, 2022)**. During the southeast monsoon, prevailing winds along the southern coast of Java are oriented in a way that favors Ekman transport. This dynamic drive a significant upwelling along the southern coast of Java, where our observations confirm high Chl-a concentrations in these waters, directly reflecting enhanced phytoplankton biomass. This localized upwelling region stands in contrast to the central ETIO, where weaker wind forcing and stronger stratification limit nutrient transport to the surface. The nutrient-rich waters brought to the surface along the southern coast of Java, characterized by elevated nitrate and phosphate concentrations, directly support a more productive ecosystem compared to the central basin.

The high intensity of upwelling along the southern Java coast is evident in the observed nutrient and chlor-a profiles. Elevated nutrient concentrations in upwelled waters contribute to higher surface productivity **(Hafiz *et al.*, 2024)**. Upwelling transports nutrients from below the nutricline, enriching the photic zone. Elevated nitrate and phosphate concentrations provide the essential macronutrients for phytoplankton growth. Phytoplankton respond rapidly to nutrient inputs, leading to elevated chlor-a concentrations near upwelling zones. This process is reflected in consistently higher surface chlor-a values along the southern Java coast than the central ETIO **(Purba *et al.*, 2019).**

The stark contrast in productivity between the upwelling zone near Java and the more stratified central ETIO illustrates the critical role of wind-driven upwelling. While

the ETIO generally exhibits oligotrophic characteristics with low surface nutrients and chlor-a, the southern Java upwelling zone acts as a productivity hotspot **(Khan *et al.*, 2024).** This is particularly important for regional fisheries, as enhanced primary productivity supports food webs, sustaining economically significant fish populations.

CONCLUSION

The results of this study provide an essential insight into the productivity of the ocean in the ETIO by analyzing nutrient dynamics, a foundational element in understanding vertical productivity. Nutrient availability, particularly nitrate, phosphate, silicate, and chlor-a, serves as a crucial indicator of ocean productivity, directly influencing primary production and the health of marine ecosystems. The findings indicate clear seasonal patterns affected by the northwest and southeast monsoons, exhibiting significant surface and subsurface dynamics variation. The distribution of nutrients, especially nitrate, phosphate, and silicate, exhibited considerable depth-dependent variability, indicating the intricate interactions of upwelling, mixing, and water mass transport processes. Temperature and salinity profiles emphasized stratification and mixing affected by monsoonal winds, whereas oxygen concentrations revealed regional variations in biological activity and physical ventilation. Combining *in-situ* observations from WOD with satellite-derived data from CMEMS improved the findings' resolution and dependability. This work highlights the essential influence of physical and chemical interactions on productivity and ecological dynamics in the ETIO. Future studies must prioritize long-term monitoring and the use of new oceanographic technology to enhance knowledge of the effects of climatic variability and anthropogenic alterations on this essential marine ecosystem.

ACKNOWLEDGMENT

The authors thank the Universitas Padjadjaran and KomitmenX Research Group. Thanks to all the committee members of the International Seminar of Indonesian Seas: Catalyst for Ocean Sustainability (ISCO) 2024, who facilitated the publication process of this manuscript until it was published in the Egyptian Journal of Aquatic Biology and Fisheries.

REFERENCES

Ayers, J. M.; Strutton, P. G.; Coles, V. J.; Hood, R. R. and Matear, R. J. (2014). Indonesian throughflow nutrient fluxes and their potential impact on Indian Ocean productivity. Geophysical Research Letters, *41*(14), 5060–5067. https://doi.org/https://doi.org/10.1002/2014GL060593

Bristow, L.A.; Mohr, W.; Ahmerkamp, S. and Kuypers, M.M.M. (2017). Nutrients that limit Growth in The Ocean. Curr. Biol., 11, 474–478. https://doi.org/10.1016/j.cub.2017.03.030

Cuypers, Y.; Bouruet-Aubertot, P.; Vialard, J. and McPhaden, M. J. (2017). Focusing of internal tides by near-inertial waves. Geophysical Research Letters, *44*(5), 2398–2406. https://doi.org/https://doi.org/10.1002/2017GL072625

Duhamel, S.; Bjorkman, K.M.; Repeta, D.J. and Karl, D.M. (2016). Phosphorus Dynamics in Biogeochemically Distinct Regions of the Southeast Subtropical Pacific Ocean. Progress in Oceanography 151, 261–274. https://doi.org/10.1016/j.pocean.2016.12.007

Emery, W. (2001). Water Types and Water Masses. Encyclopedia of Ocean Sciences, *4*, 3179–3187. https://doi.org/10.1006/rwos.2001.0108

Gordon, A. (2005). Oceanography of the Indonesian Seas and Their Throughflow. Oceanography, *18*, 14–27. https://doi.org/10.5670/oceanog.2005.01

Gulev, S. K.; Barnier, B.; Molines, J.-M.; Penduff, T. and Chanut, J. (2007). Impact of spatial resolution on simulated surface water mass transformations in the Atlantic. Ocean Modelling, *19*(3), 138–160. https://doi.org/https://doi.org/10.1016/j.ocemod.2007.07.004

Jacob, M. M.; Jones, W. L.; Santos-Garcia, A.; Drushka, K.; Asher, W. E. and Scavuzzo, C. M. (2019). Salinity Rain Impact Model (RIM) for SMAP. IEEE Journal of Selected Topics in Applied Earth Observations and Remote Sensing, *12*(6), 1679–1687. https://doi.org/10.1109/JSTARS.2019.2907275

Hafiz, M.; Widagdo, S. and Prasita, V.D. (2024). Eksistensi Upwelling Pada Fase Netral Di Perairan Selatan Jawa. Journal of Tropical Marine Research, 1–10. https://doi.org/10.30649/jrkt.v6i1.77

Kamalanathan, M.; Hillhouse, J.; Claflin, N.; Rodkey, T.; Mondragon, A.; Prouse, A.; Nguyen, M. and Quigg, A. (2021). Influence of Nutrient Status on The Response of The Diatom Phaeodactylum Tricornutum to Oil and Dispersant. PLoS One, 1;16(12): e0259506. doi: 10.1371/journal.pone.0259506. PMID: 34851969; PMCID: PMC8635359.

Khan, A. M.; Ilmi, M. H.; Febriani, C.; Sidik, T. D.; Azizah, F. N.; Ramadhanti, D. S. and Purba, N. P. (2024). Variability of biophysical parameters during La Niña condition in the Eastern Region of the Indian Ocean. Journal of Sea Research, *201*, 102533.

Labiosa, R.G.; Arrigo, K.R.; Genin, A.; Monismith, S.G. and Dijken, G. (2003). The Interplay Between Upwelling And Deep Convective Mixing In Determining The Seasonal Phytoplankton Dynamics In The Gulf Of Aqaba: Evidence from SeaWiFS and MODIS. Journal of Limnology and Oceanography, 48(6), 2355–2368.

Lee, T.; Fukumori, I.; Menemenlis, D.; Xing, Z. and Fu, L.-L. (2002). Effects of the Indonesian Throughflow on the Pacific and Indian Oceans. Journal of Physical Oceanography, *32*(5), 1404–1429. https://doi.org/https://doi.org/10.1175/1520-0485(2002)032<1404:EOTITO>2.0.CO;2

Makarim, S.; Sprintall, J.; Liu, Z.; Yu, W.; Santoso, A.; Yan, X.-H. and Susanto, R. D. (2019). Previously unidentified Indonesian Throughflow pathways and freshening in the Indian Ocean during recent decades. Scientific Reports, *9*(1), 7364. https://doi.org/10.1038/s41598-019-43841-z

Makwana, M. and Patnaik, U. (2024). Comparative VGP Models to Analyze the Primary Productivity in The North Indian Ocean and the Linkages With Rising Sea Surface Temperature. Continental Shelf Research, 277, 105254. https://doi.org/10.1016/j.csr.2024.105254

Maradhy, E.; Nazriel, R.S.; Sutjahjo, S.H.; Rusli, M.S.; Widiatmaka; Sondita and M.F.A. (2022). The Relationship of P and N Nutrient Contents with Chlorophyll-a Concentration in Tarakan Island Waters. IOP Conf. Series: Earth and Environmental Science, 1083, 012077, 1-7. doi:10.1088/1755-1315/1083/1/012077

Paul, A.J.; Bach, L.T.; Aristegui, J.; der Esch, E.; Hernandez-hernandez, N.; Piiparinen, J.; Ramajo, L.; Spiling, K. and Riebesell, U. (2022). Upwelled Plankton Community Modulates Surface Bloom Succession and Nutrient Availability in A Natural Plankton Assemblage. Biogeoscience, 1-20. https://doi.org/10.5194/bg-2022-44

Purba, N.P. and Khan, A.M.A. (2019). Upwelling Session In Indonesia Waters. World News of Natural Sciences, 25: 72-83

Purba, N. P.; Akhir, M. F.; Pranowo, W. S.; Subiyanto, and Zainol, Z. (2024). Seasonal Water Mass Transformation in the Eastern Indian Ocean from In Situ Observations. Atmosphere, *15*(1). https://doi.org/10.3390/atmos15010001

Purwandana, A.; Cuypers, Y.; Bouruet-Aubertot, P.; Nagai, T.; Hibiya, T. and Atmadipoera, A. S. (2020). Spatial structure of turbulent mixing inferred from historical CTD datasets in the Indonesian seas. Progress in Oceanography, *184*, 102312. https://doi.org/https://doi.org/10.1016/j.pocean.2020.102312

Purwandana, A.; Ismail, M. F. A.; Nugroho, D.; Atmadipoera, A. S. and Kampono, I. (2023). Hydrography and turbulent mixing in the Banda Sea inferred from Argo profiles. IOP Conference Series: Earth and Environmental Science, *1251*(1), 012007. https://doi.org/10.1088/1755-1315/1251/1/012007

Putriani, P. Y.; Atmadipoera, A. S. and Nugroho, D. (2019). Interannual variability of Indonesian throughflow in the Flores Sea. IOP Conference Series: Earth and Environmental Science, *278*(1), 012064. https://doi.org/10.1088/1755-1315/278/1/012064

Sarkar, D.; Sarkar, U.K.; Naskar, M.; Roy, K.; Bose, A.K.; Nag, S.K.; Karnatak, G. and Das, B.K. (2021). Effect Of Climato-Environmental Parameters On Chlorophyll-A Concentration In The Lower Ganga Basin, India. Revista de Biología Tropical, 69(1), 60-76. DOI 10.15517/rbt.v69i1.42731

Schlitzer, R. (2024). Ocean Data View. https://odv.awi.de

Schneider, N. (1998). The Indonesian Throughflow and the Global Climate System. Journal of Climate, *11*(4), 676–689. https://doi.org/https://doi.org/10.1175/1520-0442(1998)011<0676:TITATG>2.0.CO;2

Sprintall, J.; Gordon, A. L.; Koch-Larrouy, A.; Lee, T.; Potemra, J. T.; Pujiana, K. and Wijffels, S. E. (2014). The Indonesian seas and their role in the coupled ocean–climate system. Nature Geoscience, *7*(7), 487–492. https://doi.org/10.1038/ngeo2188

Susanto, R.; Waworuntu, J.; Prayogo, W. and Setianto, A. (2021). Moored Observations of Current and Temperature in the Alas Strait: Collected for Submarine Tailing Placement, Used for Calculating the Indonesian Throughflow. Oceanography, *34*. https://doi.org/10.5670/oceanog.2021.103

Tanaka, T.; Hasegawa, D.; Yasuda, I.; Yanagimoto, D.; Fujio, S.; Nakamura, H.; Inoue, R. and Nishioka, J. (2021). Enhanced vertical turbulent nitrate flux in the intermediate layer of the Kuroshio in the Tokara Strait. Journal of Oceanography, *77*(1), 45–53. https://doi.org/10.1007/s10872-020-00581-3

Taufiqurrahman, E.; Wahyudi, A. and Masumoto, Y. (2020). The Indonesian Throughflow and its Impact on Biogeochemistry in the Indonesian Seas. ASEAN Journal on Science and Technology for Development, *37*, 29–35. https://doi.org/10.29037/ajstd.596

Thorpe, S. A. and Deacon, G. E. R. (1997). Turbulence and mixing in a Scottish Loch. Philosophical Transactions of the Royal Society of London. Series A, Mathematical and Physical Sciences, *286*(1334), 125–181. https://doi.org/10.1098/rsta.1977.0112

Wyrtki, K. (1961). Scientific results of marine investigations of the South China Sea and the Gulf of Thailand, *1959-1961*.